Article

Wave-Current Impact on Shear Stress Patterns around 3D Shallow Bedforms

Julia Hopkins [1],*, Matthieu de Schipper [2], Meagan Wengrove [3] and Bruno Castelle [4]

1   Department of Civil and Environmental Engineering, Northeastern University, Boston, MA 02115, USA
2   Department of Hydraulic Engineering, Delft University of Technology, 2628 CD Delft, The Netherlands
3   Department of Civil Engineering, Oregon State University, Corvallis, OR 97331, USA
4   UMR EPOC, CNRS/Univ. Bordeaux, 33000 Bordeaux, France
*   Correspondence: j.a.hopkins@northeastern.edu

Abstract: Observations from wave basin experiments and wave-resolving numerical simulations demonstrate the effect of wave-current interaction on shear stress around a sandy mound. Observations from the wave basin show that the mound deformation rate and morphological patterns depend on the mixture of waves and currents in the incident flow conditions. A SWASH nonhydrostatic numerical model was used to expand the parameter space of wave-current conditions observed in the flume and characterize the response of the near-bed shear stress to the mound. The model was validated with observations from wave-alone, current-alone, and wave-current flume tests and then ran for a suite of numerical flow conditions which isolate the impact of the ratio of wave-current energy on the bed shear stress. Results show how the current-to-wave ratio impacts the spatial heterogeneity of shear stress across the mound, with the region of shear stress intensification around the mound and the location of the peak shear stress becoming asymmetric with more mixed wave-current flows. These results show the nonlinear response of shear stress patterns to combined wave-current flows and how these patterns may impact eventual sediment transport and mound evolution.

Keywords: wave-current interaction; wave-resolved models; wave lab experiments; bed shear stress

1. Introduction

The world's sandy coastlines are under threat from climate change, notably rising seas and increased storm intensity. Coastline longevity will depend on our ability to predict the response of shoreline environments to a climate-changed world for effective coastal management [1,2]. A common beach management strategy is nourishment, where piles of sand are placed either directly on a beach or in the nearshore seaward of a beach to be reworked and dispersed by local waves and tidal currents [3–7]. The efficacy of nourishment design relies on the predictive ability of nearshore sediment transport formulations in numerical models. Yet predicting sediment transport in three dimensions remains a challenge, especially in coastal environments where flow conditions and bathymetry are more complex than the typically-studied gently sloped, alongshore-uniform, wave-dominated beach [8].

State-of-the-art nearshore models, including Delft3D, COAWST, XBeach, and many more, can approximate wave evolution, tides, and sediment transport in shallow water [9–11]. The accuracy of these models often depends on "tuning" nonphysical parameters (e.g., a multiplicative factor applied to the bed/suspended transport) to site-specific observations, suggesting avenues for increased model skill through better sediment transport modeling [8,12,13]. The sediment transport formulas encoded into many models are functions of shear stress owing to wave and current conditions above the bed [14–17]. Capturing bed shear stress under a variety of hydrodynamic conditions is therefore critical to accurate sediment transport predictions.

Shear stress (τ) is a function of the water density ρ and the friction velocity at the bed u_* [18,19](Equation (1)):

$$\tau = \rho u_*^2 \qquad (1)$$

Calculating u_* requires vertical resolution of the (O(mm)) boundary flow layer above the bed. In situations where detailed measurements of boundary layer velocities are not possible, approximations for shear stress have been devised and tested [19–23]. Specifically, bed shear stress in industry-standard, coastal numerical models is calculated using time-averaged wave and current properties (e.g., significant wave height, peak wave and current directions) [15,24,25].

In most practical applications, these approximations are validated using sediment transport or bed evolution as a proxy. Good agreement between shear stress-derived sediment transport (or morphological evolution) and measured transport (or morphology) has been found in wave-dominated field environments with alongshore-uniform beach profiles [24,26]. Likewise, a reasonable agreement has been found in laboratory studies investigating the evolution of artificial sand mounds in wave flumes under a narrow range of wave conditions [27–29]. However, studies at field locations with combined wave-current flows generally find poor agreement between measured and modeled bed shear and associated sediment transport [30–33]. In fact, results from previous lab and field experiments show that combined wave-current flows have a nonlinear relationship to the bed shear stress [34–37]. The nature of this nonlinear interaction must be further explored for accurate numerical models of bed shear stress and by extension, sediment transport based on bed shear stress.

To gain insight into the impact of combined wave-current flows on bed shear stress, specifically spatial patterns of shear stress in the vicinity of a three-dimensional sandy bed feature, MODEX (Morphological Diffusivity EXperiment) was conducted in the summer of 2018. The experiment observed, in detail, the evolution of a sandy mound under a variety of wave, current, and combined wave-current flow conditions. For all prescribed flow conditions, MODEX produced measurements of velocities around the mound and maps of the mound's evolution over time. The resulting robust dataset of velocity observations is used here to understand how wave-current interaction influences bed shear stress patterns across a three-dimensional bedform.

Wave flume observations are used to force and validate the wave-resolving numerical model SWASH. Wave-resolving models, while computationally expensive and difficult to use in a regional context, allow for more detailed calculations of shear stress relative to wave-averaged models, as they can explicitly simulate the near-bed velocity owing to a variety of forced wave-current conditions [38]. Our results from SWASH expand the range of wave-current conditions tested in the flume experiment and isolate the impact of current-to-wave ratios on bed shear stress patterns over a 3D mound. We show here that bed shear stress differs between wave-dominated, current-dominated, and combined wave-current flows in magnitude and spatial extent. We found a nonlinear relationship between current-to-wave ratios and bed shear stress that is not explained by traditional, local flow nonlinearity metrics. Model results show the importance of capturing the spatial patterns of shear stress in combined wave-current flows to accurately predict bedform evolution in shallow water.

2. Materials and Methods

2.1. MODEX Experiment

The set of observations that comprise MODEX was acquired in seven weeks in the summer of 2018 at the Total Environmental Simulator in Hull, UK. The facilities consisted of a 6 m × 12 m flume with a wave maker on one side, a porous beach on the other, and a pump system that ran flow through the flume in the direction of wave propagation (Figure 1A). Initial bathymetric conditions in the flume (Figure 1B,C), were a 10 cm layer of flat sand (215 um diameter) over the entire bed, with a 20 cm high, 1.5 m diameter mound placed in the center underneath a gantry structure. To observe the flow and the mound evolution for all hydrodynamic conditions, a suite of instruments was placed around the

mound, using the gantry and a pole scaffolding frame in front of the mound location as a mounting point.

Prior to testing each of the nine experimental flow conditions, the sandy bed was flattened, and identical mounds were constructed using a specialized mold. The mound's shape was verified with laser scans after construction and before the basin was filled with water. The 3D Gaussian shape was chosen to track mound diffusivity following a theoretical mound diffusivity test case [39], the results of which are presented in [40]. The nine flow conditions consisting of monochromatic waves and steady current, as seen in Table 1, were then imposed on the mound for as long as it took the mound to diffuse to approximately half of its original height (measured by RPS scans). All conditions originated from one side of the flume, such that only the following wave-current flows (Tests 7–9) were simulated. All wave conditions were regular waves.

Table 1. Trial number and flow conditions, including flow rate (Q), wave height (H), and wave period (T) (more detail in [41]. Adapted with permission from [41], Copyright 2019, World Scientific). All combined wave-current flows were for waves and currents moving in the same direction. A new sandy mound was created for each test.

| Test #	Wave-Current Combination	Q (L/s)	H (m) Observed	T (s)
1	Waves only, low	0	0.098	1.0
2	Wave only, medium	0	0.12	1.2
3	Wave only, high	0	0.12	1.3
4	Currents only, high	900	0.00	0.0
5	Currents only, low	700	0.00	0.0
6	Combined, low energy	400	0.055	0.8
7	Combined, equal energy	500	0.12	1.2
8	Combined, current > wave energy	580	0.098	1.0
9	Combined, wave > current energy	420	0.12	1.3

Throughout the given experimental test (denoted by a single hydrodynamic condition), instruments around the mound measured velocities in the water column, the water level, and the morphology of the mound were diffused (see Figure 1a for locations and descriptions of instruments). For detail on post-processing of bathymetric and velocity data, see [40,41].

2.2. SWASH Model

SWASH is a hydrodynamic model which solves the nonlinear shallow water equations with non-hydrostatic pressure, and includes a κ-ϵ turbulence model [42]. It is used here to simulate the hydrodynamic conditions imposed in MODEX, to extend the spatial extent of the flow observations, and to simulate a larger range of wave-current flow conditions to build on the lab experiments.

The MODEX SWASH model is initialized with the observed initial mound bathymetry in the flume. One end of the model domain prescribes the flow with water level and velocity, the other end uses a sponge layer (for waves, here set to be 3 m wide in the alongshore direction) and discharge flow (currents, set to be the mean value of the incoming flow) to prevent reflection (Figure 1B). The along-flow sides of the flume are periodic to prevent nonphysical wave reflection in the domain. The model is otherwise run with default settings. A 6.7 cm $\times$ 6.7 cm resolution grid was used, balancing computational efficiency and accuracy (3 cm $\times$ 3 cm showed no improvement in results) The model has 8 vertical layers, each occupying a percentage of the water column to best capture dynamics near the bed across the flat bathymetry and over the mound (percent of water depth for vertical layers, in order from shallowest to deepest: 50, 40, 3, 2, 2, 1, 1, and 1).
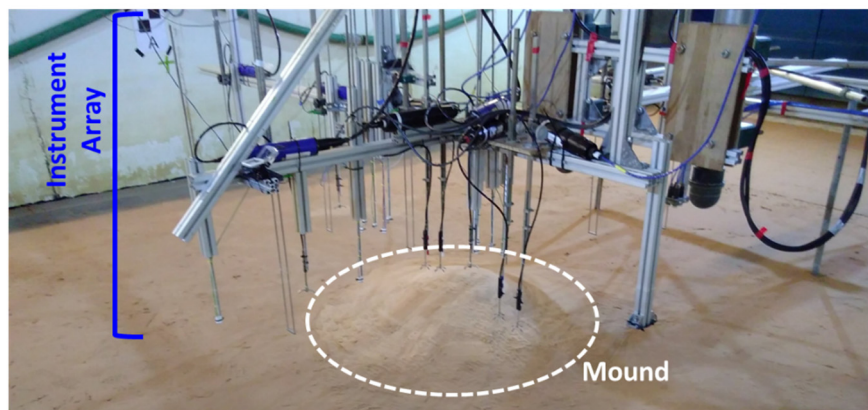
[A] MODEX Flume Setup
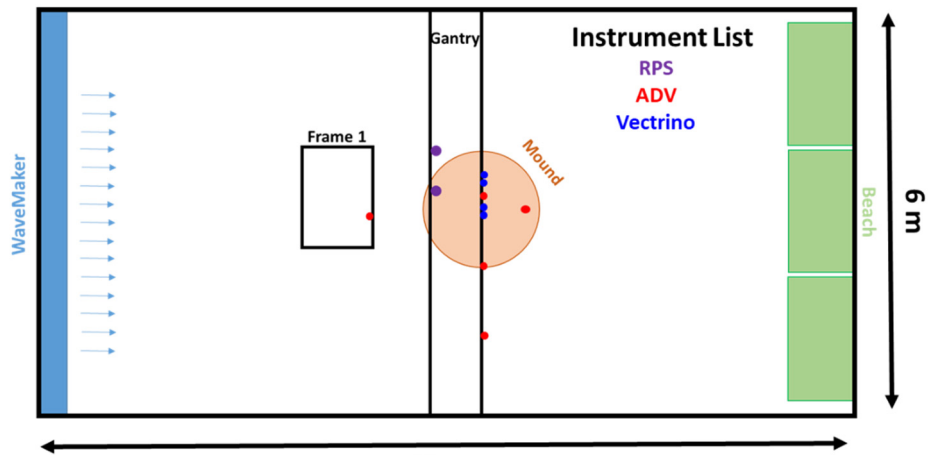
[B] SWASH Model Setup
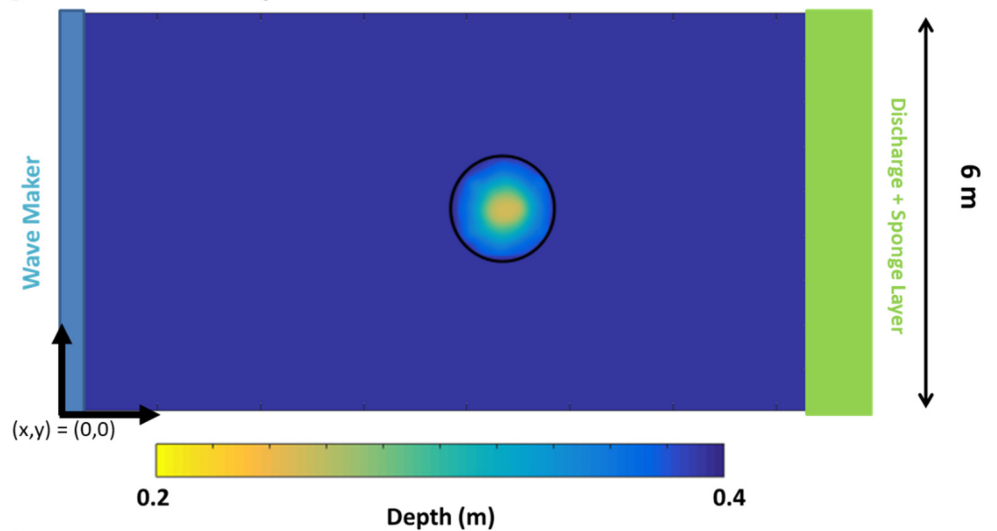
[C] Overhead shot of dry mound

Figure 1. (**A**) Experimental setup for MODEX in the 6 m × 12 m flume, the Total Environmental Simulator at the University of Hull, UK. Flow is from left to right, initiated by two pumps and a wave paddle (blue box, right). The bed of the flume was covered in 10 cm of sand except for the center, where a 20 cm tall, 1.5 m wide mound (orange circle) was constructed. Next, 40 cm of water (referenced to the flat bed) submerged both the mound and the array of instruments arranged around it, including side-scan sonars (ripple profiling sonars, RPS, and purple) and acoustic doppler velocimeters (ADV point measurements, yellow, and profiling Vectrinos, blue). (**B**) The observations from the ADVs and the RPS were used to initialize a SWASH nonhydrostatic, wave-resolving model

with a domain mimicking the MODEX experiment. Water depth was set to 40 cm (dark blue contours) with a 20 cm high mound (lighter contours) set in the center of the model domain. The shape of the mound was taken from MODEX RPS measurements. (**C**) Overhead shot of the mound (white) and instrument array (indicated with blue text) in a dry flume (prior to an experimental run).

SWASH was used to expand the parameter space of wave-current flows from the conditions observed in MODEX, adding more current-to-wave ratios and greater spatial-temporal resolution of hydrodynamic conditions around the mound. The combined wave-current tests ran in MODEX were designed for different ratios of wave-current contribution to the bed shear stress, but also had different total energies of the flow. In contrast, SWASH simulates different ratios for the same total energy. The full parameter space is shown in Table 2.

Table 2. List of flow boundary conditions generated to investigate the impact of current-to-wave ratios in the SWASH model based on conditions ran in the MODEX experiment. The first column denotes the test number the ratios were based on (compare to first column of Table 1), the second the boundary bed shear stress τ_{bound} (waves and currents combined) in MODEX for all of the subsequent conditions with varying current-to-wave ratios, the third column the number of different ratios tested in the numerical model based on the initial test conditions, and the fourth the full list of ratios explored (current-to-wave: 0 is wave-only and 1 is current-only). Bold is the ratio which matches the MODEX test, used to validate the modeled flow velocities against MODEX observations.

Base Test #	τ_{bound}	# of Ratios	Current-to-Wave Ratio (α) List
2	0.066	10	**0.01**; 0.11; 0.26; 0.35; 0.44; 0.55; 0.68; 0.76; 0.86; 0.99
3	0.072	13	**0.00**; 0.05; 0.09; 0.17; 0.28; 0.36; 0.45; 0.56; 0.63; 0.70; 0.79; 0.89; 0.96
7	0.161	13	0.00; 0.02; 0.06; 0.14; 0.25; 0.30; 0.42; 0.49; **0.57**; 0.66; 0.77; 0.84; 0.92
8	0.190	14	0.00; 0.04; 0.10; 0.19; 0.26; 0.34; 0.45; 0.52; **0.62**; 0.69; 0.74; 0.86; 0.94; 1.00
9	0.135	16	0.02; 0.05; 0.12; 0.17; 0.24; 0.30; 0.36; 0.40; **0.48**; 0.52; 0.61; 0.72; 0.78; 0.85; 0.94; 1.00

Each MODEX SWASH numerical simulation was based on measured velocity time-series in MODEX lab experiments. Three shear stress estimates were calculated for these experiments, (1) the current-only related shear stress τ_c, following Grant and Madsen (1982) [43], (2) the wave-only related shear stress τ_w, following Nielsen (1992) [44], (3) the combined shear stress, τ_{cw} using van Rijn (2007) [45]. From these, the ratio of current-to-wave contribution to the bed shear stress α was calculated as:

$$\alpha = \tau_c / (\tau_c + \tau_w) \tag{2}$$

such that $\alpha = 0$ if the flow is fully wave-dominated and $\alpha = 1$ if the flow is fully current-dominated. Using α, combined shear stress of waves and currents τ_{cw} was estimated as [45]:

$$\tau_{cw} = 0.5\rho f_{cw} U_b^2 \tag{3}$$

$$f_{cw} = \alpha\beta f_c + (1-\alpha) f_w \tag{4}$$

$$f_c = 8g / \left(18\left(\log\frac{13h}{k_s}\right)\right)^2 \tag{5}$$

$$f_w = exp\left(-6 + 5.2\left(\frac{A_w}{k_s}\right)^{-0.19}\right) \tag{6}$$

$$A_w = |U_b|T/2\pi \tag{7}$$

where ρ is the water density, f is the friction factor of either waves w or currents c, α is the current-to-wave ratio described in (2), $\beta = 1$ is a tuning parameter, h is water depth, $k_s = 15d_{50}$ where d_{50} is the sediment grain size as in van Rijn (2007), A_w is the orbital velocity amplitude based on T, wave period, and U_b, bottom velocity (measured from model results at the deepest vertical grid cell for all calculations).

The total combined shear stress τ_{bound} from MODEX (Table 2) was determined with (4)–(7) using a 60-s flow timeseries measured at the ADV located closest to the wave-maker (Figure 1). The ratio of current-to-wave contributing to τ_{bound} (calculated as in (3)) was varied to isolate the impact of wave-current interaction on the amplification of bed shear stress around the mound (see Figure 2) and create 10–16 artificial boundary conditions for each MODEX test.
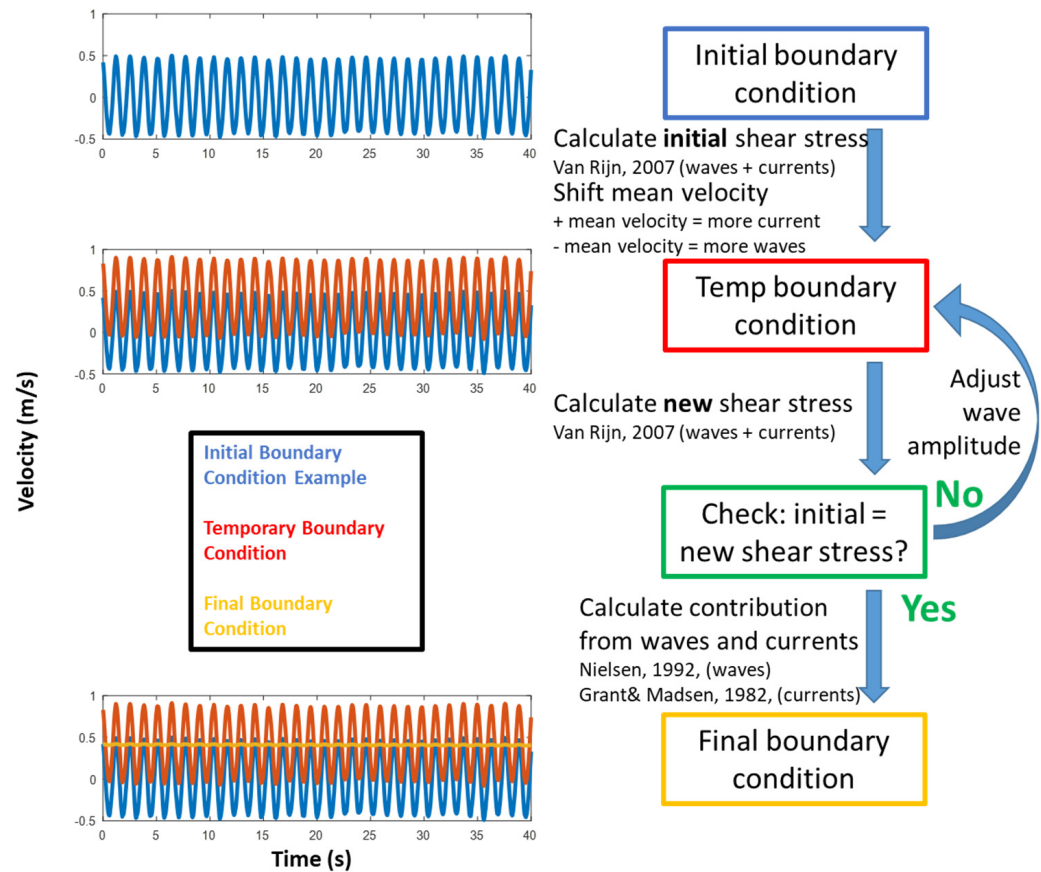

Figure 2. Workflow (right column) to generate boundary conditions (left column) for idealized SWASH runs, aiming to create a range of α values for the same total bed shear stress. Measured boundary conditions are the initial boundary conditions (left column, blue line). To vary the current contribution, these initial timeseries were shifted by adding or subtracting mean flow (left column, red line). The oscillatory component of the flow ("waves") was then adjusted iteratively until the new boundary condition (left column, yellow line) had the same (within 0.5–1%) total shear stress τ_{bound} (combined waves and currents) as the initial boundary condition (blue). The column to the right outlines the iterative workflow to calculate each successive boundary condition from the initial, observed timeseries. The contribution of waves and currents was calculated following [43,44] based on good agreement between observed and calculated bed shear stress for following waves and currents in prior lab experiments [23]. The example workflow shown here illustrates a transformation from waves-alone (blue) to current-alone (yellow) boundary flow conditions.

These new, artificial boundary conditions were fed into SWASH and ran over the initial mound profile to examine different current-to-wave ratios α with similar combined shear stress estimates (Table 2, column 4). SWASH outputs velocity and water level every second at every point in space around the simulated mound. The outputs were used to calculate the combined bed shear stress τ_{cw} around and on top of the mound using (3)–(7). All terms can be explicitly calculated from SWASH runs: the bottom velocity from the deepest grid point in the vertical, the period from the timeseries of velocity oscillation,

the water depth output from the model at every grid point, and the sediment grain size identical to MODEX and the SWASH runs.

2.3. Model Analysis

SWASH depth-averaged flow results were validated against velocity observations (Figure 3A–E) at the five ADV locations (Figure 1A, yellow dots, and Figure 3F) showing good agreement between the model and data at these locations.
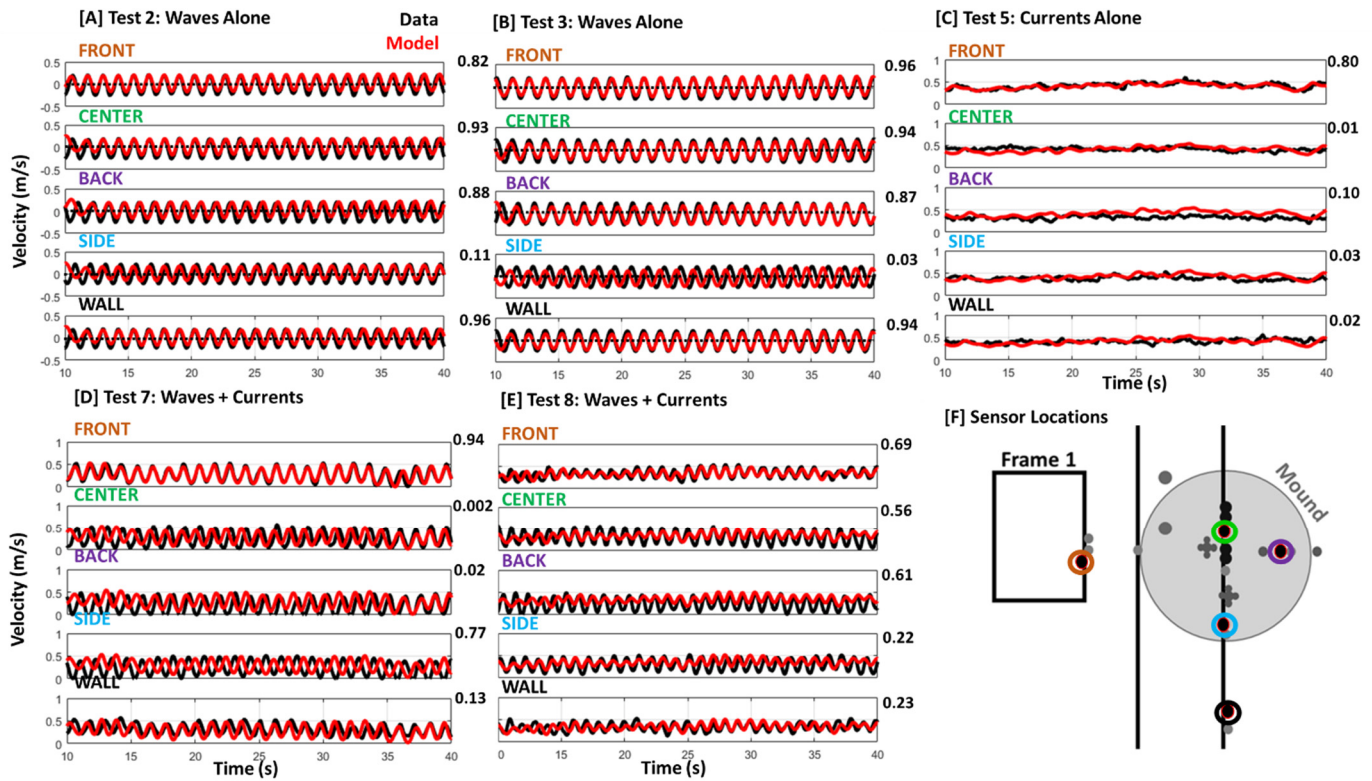

Figure 3. Data (black line)—model (red line) comparison for a series of SWASH runs based on initial conditions in the tests (Table 1) in MODEX. Model runs included waves-alone ((**A**,**B**), dashed line indicates zero-crossing), currents-alone (**C**), and wave-current combined (**D**,**E**). For each test condition, the five vertical panels show time (x-axis) vs. along-flume velocity (y-axis) at five locations within the flume (marked around the mound in colored circles in (**F**) and labeled above each timeseries plot). R^2 values are at the upper right hand of each subplot indicating goodness of fit.

For all MODEX tests used as the basis for SWASH runs seen in Figure 3, the model captures the velocity amplitude at all sensor locations. The phase and amplitude of the velocity is captured immediately around the mound ('center', 'side' and, 'back' locations in Figure 3A–E). The amplitude is also comparable between model and data at the ADVs to the side of the mound and the flume, though phase shifts between model and data are also evident (see SIDE and WALL in Figure 3A–E). It is possible that boundary effects are present in the observations which are not also captured in the model (as SWASH was ran with periodic side boundary conditions to avoid wave reflection). Further, the model may not capture flow transformation owing to subtle bathymetric features apparent in the flume but not the model (edges of the mound were smoothed in the model for numerical stability, for instance, and the model considers an ideally smoothed bed). The good agreement between flow amplitude at all locations and the phase of the oscillations at most locations indicates that the model performs well in simulating the MODEX flows around and across the mound.

Model results were also compared with two locations outfitted with ADV profilers (Figure 3, blue dots) measuring near-bed velocity. These were used to calculate bed

shear stress using van Rijn (2007) and then compared to bed shear stress calculated using simulated velocities at the same depth and location from SWASH. Figure 4 shows the resulting shear stress and amplification from the side to the top of the mound using the ADV profilers for four MODEX test cases (two wave-only, two wave-current).
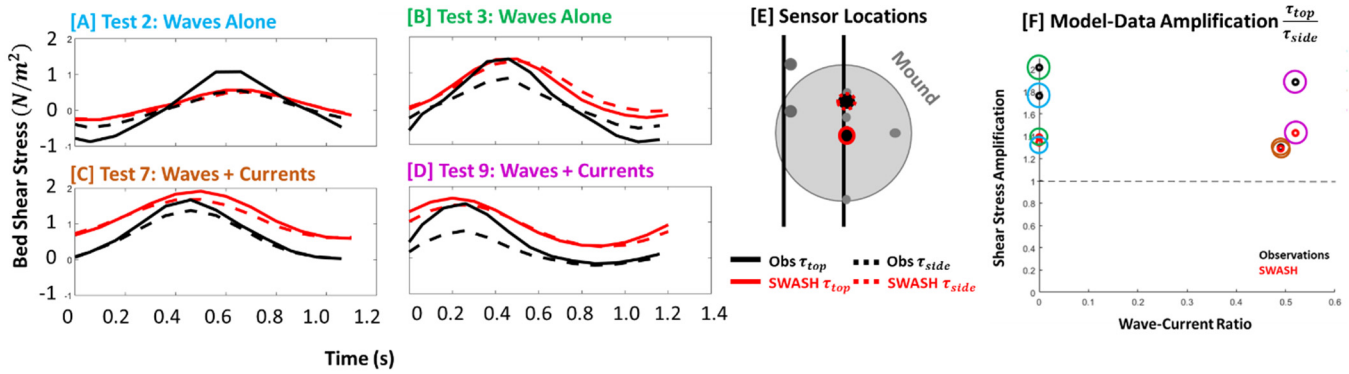
Figure 4. (**A**–**D**) Time vs bed shear stress both measured (black) and modeled (red) above the mound at the center of the mound (solid line) and the side (dashed link), with locations shown in (**E**). The bed shear stress is averaged over a wave period for each test. The phase and the magnitude of the shear stress at the bed is captured by the model with small deviations, notably in the trough of the waves. (**F**) shows current-to-wave ratio (x-axis) vs shear stress amplification (y-axis) from the side to the top of the mound between observations (black) and SWASH simulations (red) for the four test cases colored (**A**–**D**). This comparison shows similar amplification patterns from side to top of the mound, and from wave-alone to wave-current runs (higher amplification for wave-alone compared to wave-current). A current-to-wave ratio of 0 indicates wave dominant and 1 indicates current dominant.

The comparison between the model and data for the ADV profilers shows similar temporal fluctuations in bed shear stress values over a wave period. The bed shear stress is the least skillful in the trough of a wave, but the phase and magnitude are comparable between model and data (Figure 4A–D). In all cases modeled, the shear stress on the top of the mound is greater than the shear stress on the side (Figure 4F). The comparison further shows agreement in how the shear stress amplification changes as the current-to-wave ratio increases, with the amplification decreasing from side to top in both model and data. Although the ADV profilers were only located at two points around the mound, the similarities shown here suggest that SWASH has some skill in simulating the near-bed velocities used to calculated shear stress.

SWASH flow conditions were used to investigate the amplification of shear stress around a three-dimensional mound in combined wave-current flows and the role of quantifiable nonlinear wave factors in generating this amplification. All parameters were calculated using the wave-resolved flow output from the model.

For the runs with oscillatory motion, efforts to quantify wave nonlinearity center on calculating wave skewness Sk, wave asymmetry As, the combination ("nonlinear parameter" B [46]), and the Ursell number Ur, a traditional indicator of wave nonlinearity (8)–(11). For the runs with oscillatory motion, efforts to quantify wave nonlinearity center on calculating wave skewness Sk, wave asymmetry As, the combination ("nonlinear parameter" B [46]), and the Ursell number Ur, a traditional indicator of wave nonlinearity (8)–(11).

$$Sk = \frac{\overline{(u - \overline{u})^3}}{u_{rms}^3} \tag{8}$$

$$As = \frac{\mathfrak{F}(\mathcal{H}(u))^3}{u_{rms}^3} \tag{9}$$

$$B = sqrt(Sk^2 + As^2) \tag{10}$$

$$Ur = \frac{H_s\lambda^2}{h^3} \tag{11}$$

where u is the depth-averaged velocity, $\mathcal{H}$ is the Hilbert transform, the overbar denotes a time-average, H_s is the significant wave height, λ is the wavelength, and h is the water depth.

These properties were phase-averaged to compare with the bed shear stress amplification. This amplification τ_{amp} is calculated as:

$$\tau_{amp} = \frac{\tau_{cw}}{\tau_{flat}} \tag{12}$$

where τ_{cw} is the bed shear stress at each grid point from (3) and τ_{flat} is the bed shear stress from (3) averaged over a 1 m × 6 m rectangle located upstream of the mound (1 m in the along-flume direction, 6 m in the cross-flume direction). The amplification quantity τ_{amp} highlights how τ_{cw} changes as the flow passes over the mound relative to the bed shear stress over the flat bed before the mound, isolating the effect of the bathymetry on an otherwise uniform flow field. All flow properties defined in (8)–(11) were compared to τ_{amp} for each wave-current condition to determine the goodness-of-fit (R^2 value) between shear stress and the property.

3. Results

Current-to-Wave Ratios and Amplified Bed Shear Stress

The shear stress at the bed for all model runs is highest on the mound. Figure 5 shows the relationship between current-to-wave ratio α and bed shear stress calculated for a series of SWASH model runs at the crest of the mound. The results show that the bed shear stress is highest with combined wave-current flows, though the highest mean shear stress, which can be almost five-fold the boundary conditions (Figure 5A, notably blue dots), occurs closer to a current-to-wave ratio of 0.5, while the highest maximum shear stress (Figure 5B) over a wave period occurs at a ratio closer to 0.3. These results are consistent between simulations with different boundary shear stress conditions (Figure 5, colors) and with previous results showing how combined wave-current interactions enhance the bed shear stress relative to waves alone or currents alone [16,17]. Building on previous results, this study maintains constant shear boundary conditions as the ratio of waves-to-currents changes in the flow, resulting in a relationship dependent solely on the current-to-wave ratio.

The current-to-wave ratio likewise impacts the interaction of the flow with the mound. Figure 5 shows the amplification of the flat bed shear stress as the flow passes over the mound crest, both for mean shear stress averaged over a wave period (Figure 5C) and for maximum shear stress over a wave period (Figure 5D). The mean and maximum shear stress amplification have similar trends, whereby flows with more current are shown to have stronger shear stress amplification over the mound crest relative to flows with more waves.

These relationships are nonlinear, so we tested a number of common nonlinear flow parameters (Table 3) to best explain either the shear stress at the crest or the shear stress amplification from the flat bed to the mound crest. The nonlinear parameters are commonly used to describe nonlinear wave shapes, and as such, we do not anticipate that they will work for current-only flow. However, wave-current interaction has been shown to impact wave shape [25], which could provide an indication of how the bed shear stress changes relative to observable surface wave characteristics. The parameters tested were calculated from the surface waveforms simulated in SWASH (Equations (8)–(11)) at both the flat bed in front of the mound and the crest of the mound, where the shear stress was highest in all tests. The results from these correlations are discussed below.
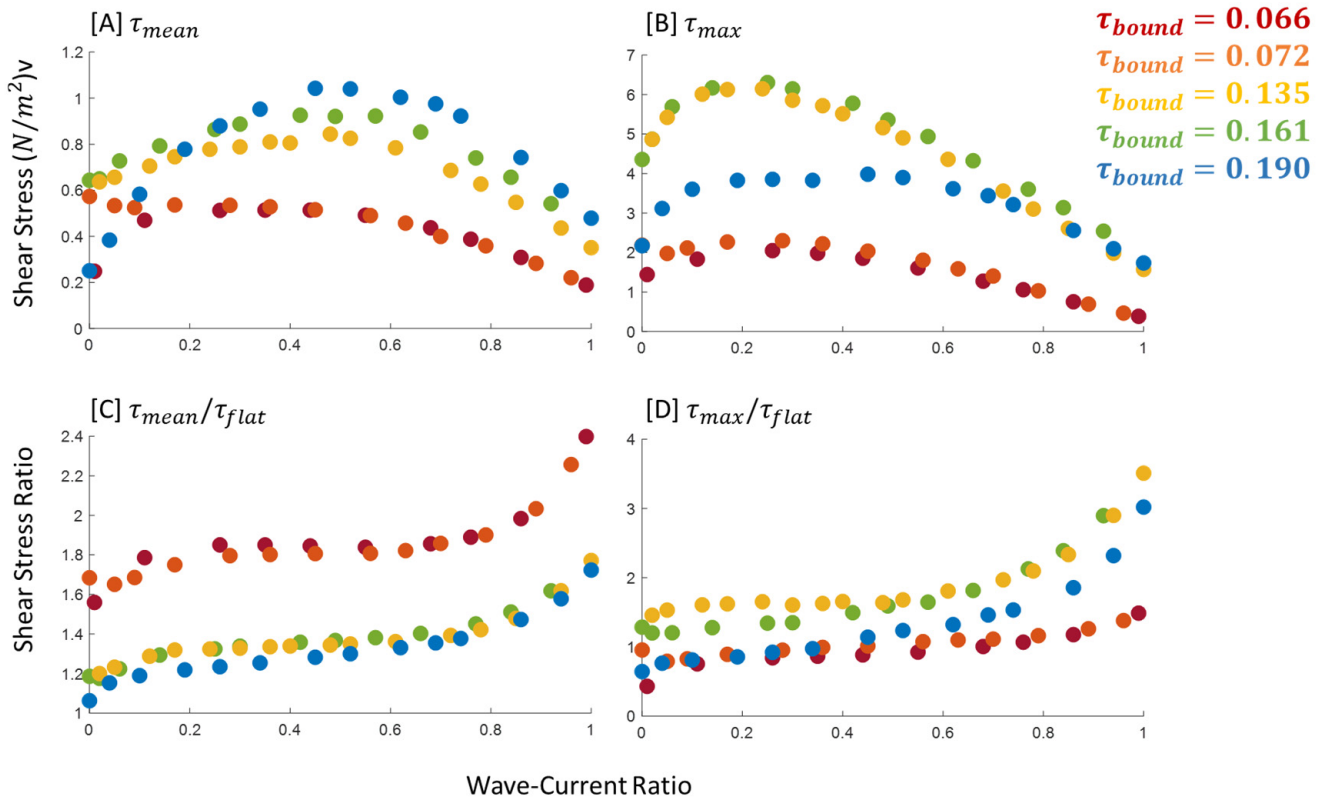
Figure 5. Current-to-wave ratio (x-axis) vs. bed shear stress (y-axis) on the top of the mound (mound crest) for (**A**) shear stress averaged over wavelength, (**B**) maximum shear stress over a water wavelength, (**C**) the amplification of the mean shear stress at the mound crest relative to the flatbed, and (**D**) the amplification of the maximum shear stress at the mound crest relative to the flatbed before the mound. The five colors indicate increasing model boundary shear stress (red is lower; blue is higher), which was kept constant for each current-to-wave ratio. Note, the y-scale in each panel is not uniform. A current-to-wave ratio of 0 indicates wave dominance and 1 indicates current dominance.

Table 3. R^2 values for linear correlations between nonlinear parameters for each wave-current condition (left column) and shear stress before the mound (τ_{flat}) and how it compares to shear stress at the mound crest (top row).

Property Name	τ_{flat}	Crest τ_{max}/τ_{flat}	Crest τ_{mean}/τ_{flat}
Skewness	0.23	0.49	0.26
Asymmetry	0.10	<0.01	<0.01
B	0.22	0.24	0.16
Ursell	0.27	0.48	0.09

4. Discussion

*Controls on Spatial Bed Shear Stress Amplification*

The shear stress averaged over time at the mound crest peaks with combined wave-current flows is similar to the maximum shear stress (Figure 5A,B). This suggests that combined wave-current flows will have higher rates of sediment transport relative to wave-alone or current-alone flows. The patterns of evolution at the mound, however, depend on how the shear stress changes from the flat bed to the mound crest. Simulations show that shear stress increases by as much as 50% at the crest of the mound for predominantly current forcing (Figure 5C,D). The mean shear stress (Figure 5C) is always higher at the mound crest relative to the flat bed. The maximum shear stress (Figure 5D), however, does not increase over the mound until currents dominate, especially if the boundary combined shear stress is at the lower end of the range simulated (red and orange dots, Figure 5D).

These trends of amplification from flat bed to mound crest are nonlinear, yet they do not appear to be captured by typical surface nonlinear parameters (Table 3). Local nonlinear parameters, such as wave skewness, asymmetry, or the combination of the two captured in the term B, and general wave nonlinear metrics, such as the Ursell number Ur do not account for the response of the bed shear stress to the presence of a mound in combined wave-current flows (Table 3). As a result, we analyzed our results with nontraditional parameters to better understand how wave-current interaction impacts bed shear stress.

SWASH simulations revealed a distinct spatial pattern in bed shear stress owing to different current-to-wave ratios, one of which was more symmetric with waves-alone and less symmetric with wave-current or current-alone flow. The asymmetry across the mound (in the direction of flow) was calculated using the continuous symmetry measure (CSM) [47], developed to detect deformation around a prescribed central axis. In this application, the metric was calculated as:

$$CSM = \frac{1}{n}\Sigma_1^n \left|m_i' - m_i\right|^2 \tag{13}$$

where m_i denotes the true value of shear stress amplification τ_{amp} across the mound at point i in space and m_i' is the corresponding symmetric shear stress amplification value across the mound. The symmetric value is determined by averaging the real values across a central axis, taken here to be the along-flume center of the mound (see the dashed black line in Figure 6).
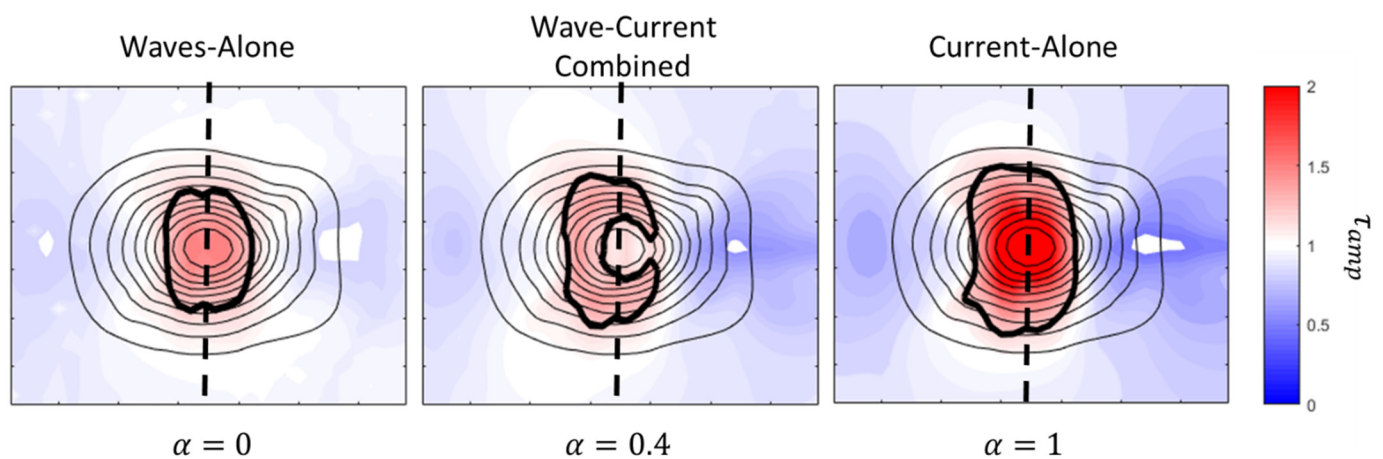
Figure 6. Illustration of symmetry in bed shear stress amplification τ_{amp} (colored contours, red is amplification above the flat bed shear stress, blue is de-amplification below the flat bed shear stress) in the along-flume direction relative to the center of the mound (dashed black line) for three current-to-wave ratios α using SWASH results from Exp 3 averaged over a wave period. The solid thick black line highlights the transition at the bed at the crest of the mound to values of shear stress higher than the flat bed shear stress seen upstream of the mound. The thin black lines are depth contours indicating the location of the mound. A current-to-wave ratio (α) of 0 indicates wave dominance and 1 indicates current dominance.

Applying the CSM to the patterns of shear stress across the peak of the mound (in the along-flume direction) for all SWASH runs shows that wave-alone flows are the most symmetric (i.e., low CSM values), a combination of waves and currents is the least symmetric, and current-alone flows tend to be somewhere in between (Figure 7).
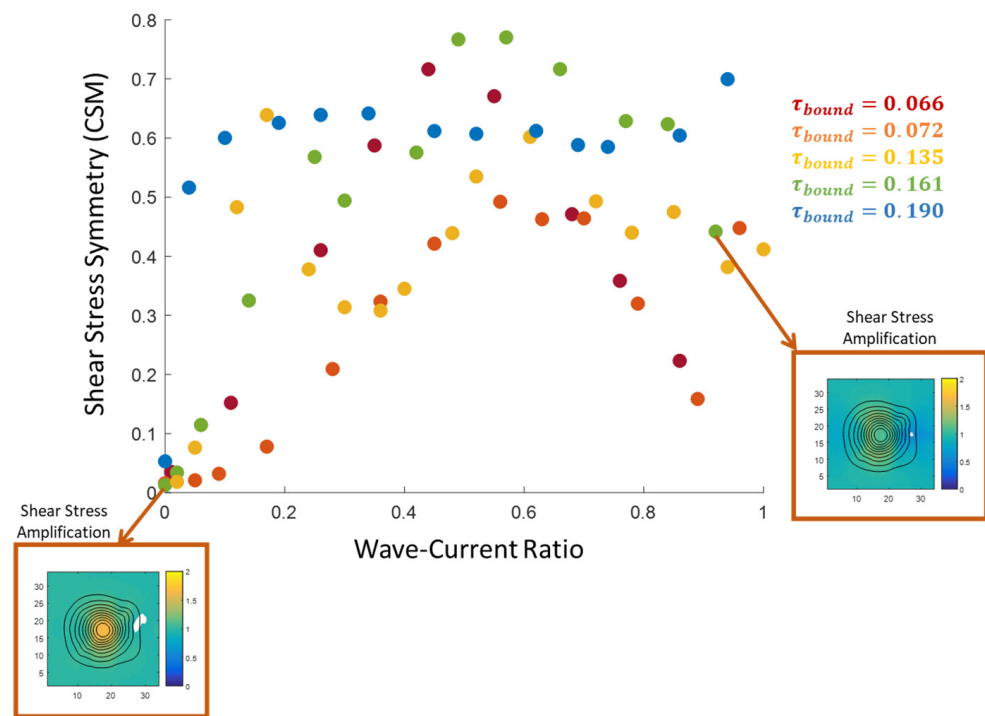
Figure 7. Values of the continuous symmetry measurement (y-axis) for each SWASH test case (colored dots, legend in upper right, values for τ_{bound} as seen in Table 2) vs. current-to-wave ratio α (x-axis). The insets pointing to specific tests show planar maps of τ_{amp} across the mound (colored contours) overlaid on depth (black contours) for Test 3, both wave-only (lower left corner) and combined wave-current (lower right corner). A CSM value of 0 indicates symmetry. A current-to-wave ratio of 0 indicates wave dominance and 1 indicates current dominance.

Figure 7 illustrates how τ_{amp} spatial patterns are most symmetric around the crest of the mound for wave-only flows, with the symmetry metric CSM for bed shear stress amplification almost zero (most symmetric) for these conditions. The spatial patterns become more asymmetric (increased CSM) as current is added to the flow, with the regions of shear stress amplification no longer clustered around the crest of the mound. Notably, conditions with small total shear stress showed strong asymmetry values even for low wave current ratios (Figure 7, red dots). This symmetry, or lack thereof, is important to understand because it dictates how the mound will evolve over time. More symmetric shear stress amplification will lead to symmetric deformation (akin to a diffusive process), and thus a simpler morphological evolution prediction. Asymmetric shear stress patterns will alter the shape of the bedform and complicate predictions of morphological evolution.

Symmetric vs. asymmetric behavior for wave or flow forcing versus combined forcing could in part be explained by how much and if the flow reverses over time. Wave-alone conditions, for instance, have flow reversals every wave period. Adding current to the flow reduces and eventually eliminates the flow reversal, potentially increasing the asymmetry in bed shear stress patterns across the mound. To investigate this further, a simple parameter v_p, the percent of the time the flow velocity is negative for a given model run, was calculated. The parameter v_p was zero for all current-dominated runs (all flow was in one direction), but for runs with sufficient wave contribution, an increase in v_p, or flow symmetry in time (across the zero-crossing), matches a decrease in CSM, or flow asymmetry in space (Figure 8).
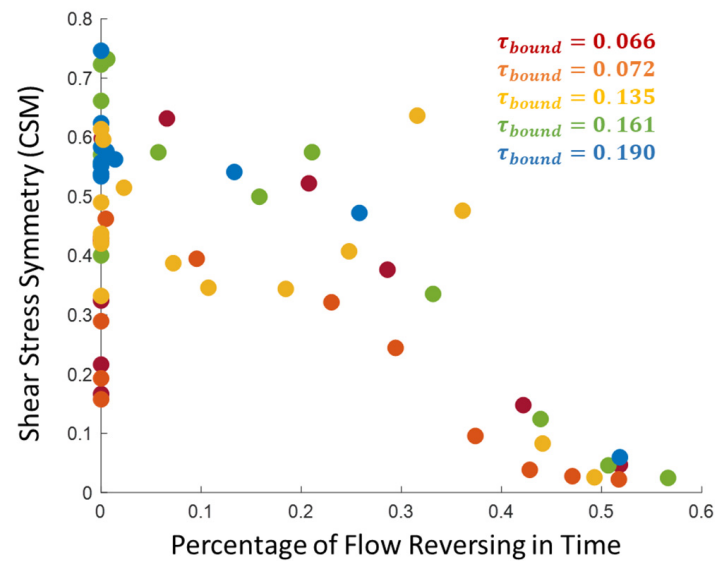
Figure 8. Values of the continuous symmetry measurements (y-axis) for each SWASH test case (colored dots, legend in upper right) vs. v_p, the percentage of flow reversing over the zero-crossing in time (x-axis). For all α with some flow reversal (all colored dots for which $v_p > 0$) the asymmetry across the mound decreases with more wave-dominated flows.

The relationship between symmetry and flow reversal in Figure 8 shows that wave-alone flows have more symmetric shear stress patterns around the mound, and adding more current to the flow increases the asymmetry. These results have some dependence on the total shear stress forced at the boundary (colors in Figures 7 and 8), with stronger flow conditions generally having less symmetric patterns than weaker flow conditions for the same current-to-wave ratio.

The spatial asymmetry of shear stress amplification influences how the mound evolves over time, with a more radially symmetric diffusion pattern observed for waves alone during MODEX, and more skewed patterns observed for all other flow conditions. The temporal asymmetry (specifically flow reversal over a wave period) correlates to spatial symmetry in the case of more wave-influenced flow conditions. The range of shear stress behaviors captured by the model and the lab observations are shown here to be dependent on the ratio of wave-current influence on the flow, suggesting that wave-averaged parameters which do not account for the mixture of wave-current influence may not capture the correct impact of flow on shear stress over bathymetric features, such as a mound.

5. Conclusions

SWASH simulations exploring the range of current-to-wave ratios α for different combined bed shear stresses were used here to show the impact of wave-current interaction on the response of bed shear stress to a sandy mound. This study uses an experimentally validated wave-resolving model to explore the parameter space of wave-current interaction. Simulation results show that the flat bed shear stress can almost double symmetrically or asymmetrically around the mound crest depending on the current-to-wave ratio and despite identical boundary shear stress. These effects are not predicted by typical nonlinear parameters, but instead relate to wave-resolved flow oscillation and spatial asymmetry.

Future studies, both observational and numerical, with a range of bathymetric shapes, different depths, and wave-current conditions are necessary to develop a new nondimensional parameter to capture the nonlinear effects of wave-current interaction on bed shear stress, and thus give wave-averaging models improved parameterizations to predict bed shear stress and subsequent bathymetric evolution in complex coastal environments. This research suggests that numerical studies in areas with complex wave-current flows may need to consider the three-dimensionality of the shear stress around bedforms. More re-

search is needed to understand the magnitude of this complexity around multiple bedforms at larger (meters) scales in the field.

References

1. Vousdoukas, M.; Ranasinghe, R.; Mentaschi, L.; Plomaritis, T.A.; Athanasiou, P.; Luijendijk, A.P.; Feyen, L. Sandy Coastlines under Threat of Erosion. *Nat. Clim. Chang.* **2020**, *10*, 260–263. [CrossRef]
2. Cooper, J.A.G.; Masselink, G.; Coco, G.; Short, A.D.; Castelle, B.; Rogers, K.; Anthony, E.; Green, A.N.; Kelley, J.T.; Pilkey, O.H.; et al. Sandy Beaches Can Survive Sea-Level Rise. *Nat. Clim. Chang.* **2020**, *10*, 993–995. [CrossRef]
3. Stronkhorst, J.; Huisman, B.; Giardino, A.; Santinelli, G.; Santos, F.D. Sand Nourishment Strategies to Mitigate Coastal Erosion and Sea Level Rise at the Coasts of Holland (The Netherlands) and Aveiro (Portugal) in the 21st Century. *Ocean Coast. Manag.* **2018**, *156*, 266–276. [CrossRef]
4. Bergillos, R.J.; Rodríguez-Delgado, C.; Ortega-Sánchez, M. Advances in Management Tools for Modeling Artificial Nourishments in Mixed Beaches. *J. Mar. Syst.* **2017**, *172*, 1–13. [CrossRef]
5. Luijendijk, A.P.; Ranasinghe, R.; de Schipper, M.A.; Huisman, B.A.; Swinkels, C.M.; Walstra, D.J.R.; Stive, M.J.F. The Initial Morphological Response of the Sand Engine: A Process-Based Modelling Study. *Coast. Eng.* **2017**, *119*, 1–14. [CrossRef]
6. Stive, M.J.F.; de Schipper, M.A.; Luijendijk, A.P.; Aarninkhof, S.G.J.; van Gelder-Maas, C.; van Thiel de Vries, J.S.M.; de Vries, S.; Henriquez, M.; Marx, S.; Ranasinghe, R. A New Alternative to Saving Our Beaches from Sea-Level Rise: The Sand Engine. *J. Coast. Res.* **2013**, *290*, 1001–1008. [CrossRef]
7. de Schipper, M.A.; Ludka, B.C.; Raubenheimer, B.; Luijendijk, A.P.; Schlacher, T.A. Beach Nourishment Has Complex Implications for the Future of Sandy Shores. *Nat. Rev. Earth Environ.* **2020**, *2*, 70–84. [CrossRef]
8. Amoudry, L.O.; Souza, A.J. Deterministic Coastal Morphological and Sediment Transport Modeling: A Review and Discussion. *Rev. Geophys.* **2011**, *49*, 1–21. [CrossRef]
9. Lesser, G.R.; Roelvink, J.A.; van Kester, J.A.T.M.; Stelling, G.S. Development and Validation of a Three-Dimensional Morphological Model. *Coast. Eng.* **2004**, *51*, 883–915. [CrossRef]
10. Warner, J.C.; Armstrong, B.; He, R.; Zambon, J.B.; Sherwood, C.R.; Signell, R.P.; Harris, C.K.; Arango, H.G. Development of a Coupled Ocean–Atmosphere–Wave–Sediment Transport (COAWST) Modeling System. *Comput. Geosci.* **2008**, *34*, 230–244. [CrossRef]
11. Roelvink, D.; Reniers, A.J.H.M.; Van Dongeren, A.; Van Thiel de Vries, J.; Lescinski, J.; McCall, R. *XBeach Model Description and Manual*; Unesco-IHE Institute for Water Education, Deltares and Delft University of Technology: Delft, The Netherlands, 2010.
12. Lu, Y.; Li, S.; Zuo, L.; Liu, H.; Roelvink, J.A. Advances in Sediment Transport under Combined Action of Waves and Currents. *Int. J. Sediment Res.* **2015**, *30*, 351–360. [CrossRef]

13. Ranasinghe, R. On the Need for a New Generation of Coastal Change Models for the 21st Century. *Sci. Rep.* **2020**, *10*, 2010. [CrossRef] [PubMed]

14. van Rijn, L.C. *General View on Sand Transport by Currents and Waves: Data Analysis and Engineering Modelling for Uniform and Graded Sand (TRANSPOR 2000 and CROSMOR 2000 Models)*; Deltares (WL): Delft, The Netherlands, 2000.

15. Soulsby, R.L.; Damgaard, J.S. Bedload Sediment Transport in Coastal Waters. *Coast. Eng.* **2005**, *52*, 673–689. [CrossRef]

16. Soulsby, R.L.; Clarke, S. *Bed Shear-Stresses Under Combined Waves and Currents on Smooth and Rough Beds*; HR Wallingford: Wallingford, UK, 2005; Volume 1905.

17. Drake, D.E.; Cacchione, D.A.; Grant, W.D. Shear Stress and Bed Roughness Estimates for Combined Wave and Current Flows over a Rippled Bed. *J. Geophys. Res.* **1992**, *97*, 2319. [CrossRef]

18. Longuet-Higgins, M.S.; Stewart, R.W. Radiation Stresses in Water Waves; a Physical Discussion, with Applications. *Deep. Res. Oceanogr. Abstr.* **1964**, *11*, 529–562. [CrossRef]

19. Grant, W.D.; Madsen, O.S. Combined Wave and Current Interaction with a Rough Bottom. *J. Geophys. Res.* **1979**, *84*, 1797–1808. [CrossRef]

20. Fredsøe, J.; Andersen, K.H.; Mutlu Sumer, B. Wave plus Current over a Ripple-Covered Bed. *Coast. Eng.* **1999**, *38*, 177–221. [CrossRef]

21. Raushan, P.K.; Singh, S.K.; Debnath, K.; Mukherjee, M.; Mazumder, B.S. Distribution of Turbulent Energy in Combined Wave Current Flow. *Ocean Eng.* **2018**, *167*, 310–316. [CrossRef]

22. Teles, M.J.; Pires-Silva, A.A.; Benoit, M. Numerical Modelling of Wave Current Interactions at a Local Scale. *Ocean Model.* **2013**, *68*, 72–87. [CrossRef]

23. Wengrove, M.E.; Foster, D.L.; Lippmann, T.C.; de Schipper, M.A.; Calantoni, J. Observations of Bedform Migration and Bedload Sediment Transport in Combined Wave-Current Flows. *J. Geophys. Res. Ocean.* **2019**, *124*, 4572–4590. [CrossRef]

24. Williams, J.J.; Rose, C.P.; Thorne, P.D.; O'Connor, B.A.; Humphery, J.D.; Hardcastle, P.J.; Moores, S.P.; Cooke, J.A.; Wilson, D.J. Field Observations and Predictions of Bed Shear Stresses and Vertical Suspended Sediment Concentration Profiles in Wave-Current Conditions. *Cont. Shelf Res.* **1999**, *19*, 507–536. [CrossRef]

25. Wolf, J.; Prandle, D. Some Observations of Wave–Current Interaction. *Coast. Eng.* **1999**, *37*, 471–485. [CrossRef]

26. Fernández-Mora, A.; Calvete, D.; Falqués, A.; De Swart, H.E. Onshore Sandbar Migration in the Surf Zone: New Insights into the Wave-Induced Sediment Transport Mechanisms. *Geophys. Res. Lett.* **2015**, *42*, 2869–2877. [CrossRef]

27. Smith, E.R.; Mohr, M.C.; Chader, S.A. Laboratory Experiments on Beach Change Due to Nearshore Mound Placement. *Coast. Eng.* **2017**, *121*, 119–128. [CrossRef]

28. Stansby, P.K.; Huang, J.; Apsley, D.D.; García-Hermosa, M.I.; Borthwick, A.G.L.; Taylor, P.H.; Soulsby, R.L. Fundamental Study for Morphodynamic Modelling: Sand Mounds in Oscillatory Flows. *Coast. Eng.* **2009**, *56*, 408–418. [CrossRef]

29. Ruol, P.; Martinelli, L.; Favaretto, C.; Scroccaro, D. Innovative Sand Groin Beach Nourishment with Environmental, Defense and Recreational Purposes. In Proceedings of the The 28th International Ocean and Polar Engineering Conference, Sapporo, Japan, 30 July 2018; International Society of Offshore and Polar Engineers: Sapporo, Japan, 2018.

30. Egan, G.; Cowherd, M.; Fringer, O.; Monismith, S. Observations of Near-Bed Shear Stress in a Shallow, Wave- and Current-Driven Flow. *J. Geophys. Res. Ocean.* **2019**, *124*, 6323–6344. [CrossRef]

31. Zhu, Q.; van Prooijen, B.C.; Wang, Z.B.; Ma, Y.X.; Yang, S.L. Bed Shear Stress Estimation on an Open Intertidal Flat Using in Situ Measurements. *Estuar. Coast. Shelf Sci.* **2016**, *182*, 190–201. [CrossRef]

32. Kalligeris, N.; Smit, P.B.; Ludka, B.C.; Guza, R.T.; Gallien, T.W. Calibration and Assessment of Process-Based Numerical Models for Beach Profile Evolution in Southern California. *Coast. Eng.* **2020**, *158*, 103650. [CrossRef]

33. van Duin, M.J.P.; Wiersma, N.R.; Walstra, D.J.R.; van Rijn, L.C.; Stive, M.J.F. Nourishing the Shoreface: Observations and Hindcasting of the Egmond Case, The Netherlands. *Coast. Eng.* **2004**, *51*, 813–837. [CrossRef]

34. Soulsby, R.L.; Humphery, J.D. Field Observations of Wave-Current Interaction at the Sea Bed. In *Water Wave Kinematics*; Springer: Dordrecht, The Netherlands, 1990; pp. 413–428.

35. Arnskov, M.M.; Fredsøe, J.; Sumer, B.M. Bed Shear Stress Measurements over a Smooth Bed in Three-Dimensional Wave-Current Motion. *Coast. Eng.* **1993**, *20*, 277–316. [CrossRef]

36. Yuan, J. Turbulent Boundary Layers under Irregular Waves and Currents: Experiments and the Equivalent-Wave Concept. *J. Geophys. Res. Ocean.* **2016**, *121*, 2616–2640. [CrossRef]

37. Moulton, M.; Elgar, S.; Raubenheimer, B. A Surfzone Morphological Diffusivity Estimated from the Evolution of Excavated Holes. *Geophys. Res. Lett.* **2014**, *41*, 4628–4636. [CrossRef]

38. Rijnsdorp, D.P.; Smit, P.B.; Zijlema, M.; Reniers, A.J.H.M. Efficient Non-Hydrostatic Modelling of 3D Wave-Induced Currents Using a Subgrid Approach. *Ocean Model.* **2017**, *116*, 118–133. [CrossRef]

39. De Vriend, H.J. Analysis of Horizontally Two-Dimensional Morphological Evolutions in Shallow Water. *J. Geophys. Res.* **1987**, *92*, 3877. [CrossRef]

40. de Schipper, M.A.; Hopkins, J.; Wengrove, M.; Saxoni, I.; Klienhans, M.; Senechal, N.; Castelle, B.; Ribas, F.; Ruessink, B.G.; Murphy, B.; et al. MODEX: Laboratory Experiment Exploring Sediment Spreading of a Mound under Waves and Currents. In Proceedings of the Coastal Sediments, 27–31 May 2019; World Scientific Pub Co Pte Lt: Singapore, 2019; pp. 511–524.

41. Hopkins, J.; de Schipper, M.A.; Wengrove, M.; De Wit, F.; Castelle, B. Observations and Numerical Model Results of Morpho-dynamic Feedback Owing to Wave-Current Interaction. In Proceedings of the Coastal Sediments 2019, 27–31 May 2019; World Scientific Pub Co Pte Lt: Singapore, 2019; pp. 553–564.
42. Zijlema, M.; Stelling, G.; Smit, P. SWASH: An Operational Public Domain Code for Simulating Wave Fields and Rapidly Varied Flows in Coastal Waters. *Coast. Eng.* **2011**, *58*, 992–1012. [CrossRef]
43. Grant, W.D.; Madsen, O.S. Movable Bed Roughness in Unsteady Oscillatory Flow. *J. Geophys. Res.* **1982**, *87*, 469. [CrossRef]
44. Nielsen, P. *Coastal Bottom Boudary Layers and Sediment Transport*; World Scientific Publishing: Singapore, 1992.
45. Van Rijn, L.C. Unified View of Sediment Transport by Currents and Waves. I: Initiation of Motion, Bed Roughness, and Bed-Load Transport. *J. Hydraul. Eng.* **2007**, *133*, 649–667. [CrossRef]
46. de Wit, F.; Tissier, M.; Reniers, A. Characterizing Wave Shape Evolution on an Ebb-Tidal Shoal. *J. Mar. Sci. Eng.* **2019**, *7*, 367. [CrossRef]
47. Chen, J.G.; Büyüköztürk, O. A Symmetry Measure for Damage Detection with Mode Shapes. *J. Sound Vib.* **2017**, *408*, 123–137. [CrossRef]